# Statistical estimation of container condensation in marine transportation between Far East Asia and Europe

Yuen, Ping Chi
Sasa, Kenji
Kawahara, Hideo
Chen, Chen

(Citation)
The Journal of Navigation,75(1):176-199

(Issue Date)
2022-01

(Resource Type)
journal article

(Version)
Accepted Manuscript

# Statistical Estimation of Container Condensation in Marine Transportation between Far East Asia and Europe

Ping Chi Yuen[a], Kenji Sasa[a,*], Hideo Kawahara[b], and Chen Chen[c]

[a]Graduate School of Maritime Sciences, Kobe University, Kobe, Japan
5-1-1, Fukae Minamimachi, Higashinada, Kobe 658-0022 JAPAN
[b]Department of Maritime Technology, Oshima National College of Maritime Technology, Yamaguchi, Japan
1091-1 Komatsu, Suo Oshima, Oshima, Yamaguchi 742-2193 JAPAN
[c]School of Navigation, Wuhan University of Technology, Wuhan, China
122 Luoshi Road, Wuhan, Hubei, 430070 CHINA
* Corresponding Author (sasa@maritime.kobe-u.ac.jp)

Abstract

Condensation inside the marine container occurs during voyages owing to weather changes. In this study, we define the condensation probability along one of the major routes for container ships between Asia and Europe. First, the inside and outside air conditions were measured on land in Japan, and a correlation analysis was conducted to derive their relationship. Second, onboard measurements were conducted for 20,000 twenty-foot equivalent unit ship to determine the variation in outside air conditions. Complicated patterns of weather change are observed with changes in latitude, sea area, and season. Third, condensation probability was estimated based on a multi-regression analysis with land and onboard measured data. The maximum condensation probability in westbound or eastbound voyages in winter is found to be approximately 50%. The condensation probability estimation method established in this study can contribute to the quantification of cargo damage risks for the planning of marine container transportation voyages.

## 1. Introduction

The intermodal shipping container was invented by the American businessman Malcom Mclean in 1956 (Levinson, 2006). Since then, containerization has facilitated global trade by decreasing transportation time and costs. In 2018, the global volume of container cargo increased by 146.4 million twenty-foot equivalent unit (TEU), and it has been forecasted to increase by 5% in 2021 (Knowler, 2019). It is undeniable that our daily lives cannot be sustained without container transportation as a global economic activity. Marine container transportation has enhanced the development of the global economy, and efficient and time-

saving transportation has become a requirement in the past decades. Furthermore, the energy efficiency design index (EEDI) has issued in the field of marine transportation since 2013. The reduction of greenhouse gas (GHG) emissions is required for the marine container transportation to satisfy the EEDI.

Many studies on optimal ship routing have been conducted in the last decades (Prpić-Oršić et al., 2012; Shoji, 2013; Maki et al., 2011; Bijlsma, 2008; Chang et al., 2016; Chou, 2017). These studies focused on the optimization of the voyage time, fuel consumption, and GHG emissions. However, during cargo operation and marine transportation, the internal air conditions of the container are influenced by changes in meteorological conditions, water content of the wooden container floor, cargo, packaging material, and other external factors. When cargo is sealed in airtight containers, the moisture inside the container turns into condensation as a result of these changes. Water droplets formed by condensation inside the container cause serious damage to the cargo. Herein, a field survey of a Japanese container terminal was also conducted. It was observed that the moisture inside the wooden container floor influences the humidity inside the container. Iejavs et al. (2016) evaluated the properties regarding the moisture permeability of cellular wood panel walls with different thicknesses and weights. Chiniforush et al. (2019) showed the effects of moisture content and temperature on the diffusion properties of glued laminated timber. Chang et al. (2020) assessed the moisture risk to cross-laminated timber based on different climate conditions, types of insulation, and application of resistant materials. These studies showed that the moisture content of wooden materials varies with the type, thickness, weight, and quality of the wood under different atmospheric conditions. All these factors contribute to the moisture inside a container. The condensation problem is simplified by considering the effects of external meteorological conditions only, because the measured results are available only for a dry box container with a plywood floor.

Studies on the issue of condensation in dry containers began in the 1970s (Imaeda et al., 1971). Weiskircher (2008) summarized the results of 6 studies based on the effects of air temperature inside a dry container during its transportation through land and sea. This literature summarized the most important and significant research on condensation; however, little progress has been made in terms of further developments to address this problem. This can be attributed to the growing market share of reefer containers in early 2000. The market share of reefer containers under refrigerated transportation increased from 50% to 80% between 2005 and 2016, while that of the reefer vessels decreased from 50% to 20%. (Castelein et al., 2020). In response to this growing trend, the focus of related studies has shifted from dry containers to reefer containers. In the case of reefer containers, the air condition can be regarded as a fluid dynamic problem to be addressed using computed fluid dynamics (CFD). However, the problem of condensation inside a dry container still remains unsolved. Studies regarding this condensation problem and the air temperature in dry containers are discussed in the following

paragraphs.

Ayyad et al. (2017) studied the change in water content of vegetable oils when transported by two different types of containers. Their results showed that thermal isolation was effective in protecting cargo from climate stress. Sharp et al. (1979) tested the insulating ability of sugarcane fiber and aluminum foil when transporting cocoa beans from Papua New Guinea to Australia. Palacios-Cabrera et al. (2007) examined the changes in the temperature, relative humidity, and moisture content of green coffee beans transported from Brazil to Italy. The coffee beans in the hold showed the highest variation in moisture content, and the regions of the container near the wall and ceiling were found to be susceptible to condensation. Excell (1989) studied the condensation problem during the transportation of refined sugar in containers from Durban to Cape Town. They found that the hot sugar had greater the probability of condensation than the cold sugar owing to the higher temperature gradient. These studies focus on evaluating the insulating ability of different materials from the viewpoint of condensation within the container. However, the internal conditions of these containers change with the external air conditions during marine transportation. The relationship between the internal and external air conditions has not been discussed in these studies.

The climate profile inside containers has also been studied in the field of transportation and applied packaging. Leinberger (2006) performed experiments to measure extreme weather conditions by installing sensors inside containers for shipments between Asia, Europe, and North America. Csavajda et al. (2019) calculated the mean statistical value of the temperature and humidity inside containers for shipments from Hungary to India, China, and South Africa. Borocz et al. (2015) and Singh et al. (2012) highlighted the importance of special packaging design for protecting cargoes against extreme climate events during navigation. Accorsi et al. (2014) measured the temperature variation inside a container during navigation from Italy to North America and Far East Asia. However, these studies did not focus on the meteorological conditions. In this study, we consider the meteorological conditions by conducting onboard measurements of outside air conditions in different seasons from Far East Asia to Europe. As it is not realistic to monitor the internal air conditions of all the containers, a new methodology should be modeled to estimate the internal air conditions from the external weather data. Meteorological conditions are measured onboard in different seasons from Far East Asia to Europe, and simple statistical models are constructed to estimate the internal air conditions of containers here.

In the field of heat conduction, Imaeda et al. (1971, 1974) measured the changes in temperature and humidity inside and outside an aluminum container and an iron container in several ports in Japan. Although these studies attempted to investigate the relationship between the external and internal conditions of containers, the experiments were limited to land measurements.

In this study, we investigated the relationship between the inside and outside conditions of

containers through sensor measurements of solar radiation, temperature, and air temperature in a 20,000 twenty-foot equivalent unit (TEU) container ship travelling between Far East Asia and Europe in May 2019. We explored the mechanism of container condensation in different sea regions, seasons, latitudes, and other factors on a time-space scale. Based on the measurements, we propose a statistical model to estimate the condensation probability by considering external weather conditions.

The rest of this paper is organized as follows. In Section 2, we describe the phenomenon of container condensation. In Section 3, we introduce the setting of the land and onboard measurements. In section 4, we report and discuss the measurements and the results of a correlation analysis of each parameter. In Section 5, we describe the multi regression modeling and discuss the estimation results of the inside air conditions for all voyages. In Section 6, we define and estimate the condensation probability for certain patterns of loading and discharging ports. Finally, in Section 7, we present the conclusions of this study.

## 2. Definition of container condensation

In general, container condensation occurs if either one of the following conditions is satisfied:

$$\text{Case 1: } T_w < D_a, \tag{1}$$

$$\text{Case 2: } D_i > T_a, \tag{2}$$

where $T_w$ [°C] is the temperature of the internal side of the container wall at the top level, $D_i$ [ºC] is the dew point temperature inside the container, $T_a$ [ºC] is the outside air temperature, and $D_a$ [ºC] is the outside dew point temperature. Case 1 occurs easily when the vessel is loaded at a port in a high-latitude region under cold weather conditions and is discharged at a port in a low-latitude region with warm weather conditions. During navigation from cold to warm regions, $T_a$ and $D_a$ increase, while $T_w$ remains almost the same in the case of poor ventilation; as a result, condensation may occur inside the container at the discharging port. Case 2 occurs easily when the vessel is loaded at a port in a low-latitude region with warm weather conditions and is discharged at port in a high-latitude region under cold weather conditions. During navigation from warm to cold regions, both $T_a$ and $D_a$ decrease, while $D_i$ remains almost the same in the case of poor ventilation; as a result, condensation is expected to occur at the discharging port.

## 3. Land and onboard measurements

In this study, we first conducted land measurements of a real-scale container to examine the relationship between the air conditions inside and outside the container. Second, we conducted onboard measurements to study the weather changes during navigation across the ocean.

### *3.1. Land measurement*

Land measurements were carried out at two different locations, as shown in Figure 1. First, measurements were carried out to determine the inside and outside air conditions, excluding solar radiation, of the real-scale dry box container shown in Figure 2 (left). The container was a 20-foot container (length: 6.058 m, width: 2.438 m, height: 2.591 m). The measurements were carried out at the Oshima National College of Maritime Technology in Yamaguchi, Japan, for several cases in summer (Cases L1–L3), fall (Cases L4–L9), and winter (Cases L10–13) in 2019 and 2020. The measurement programs are summarized in Table 1. The mounting positions of the sensors around the container are shown in Figure 2 (right). Inside the container, air temperature, humidity, and condensation were measured at multiple positions (upper, middle, and lower positions). Humidity inside the container was detected in the fall and winter seasons. Outside the container, the air temperature and humidity were measured simultaneously using thermocouples and thermo-hygrometers installed inside and outside the container, respectively. The condensation sensor is installed only for Case L-13. The measured data were recorded and transferred into a data logger every second. The solar radiation data measured by the Japan Meteorology Agency (JMA), Hiroshima, were used in this study. The weather conditions of Yamaguchi and Hiroshima were nearly the same because they are separated by only approximately 60 km.

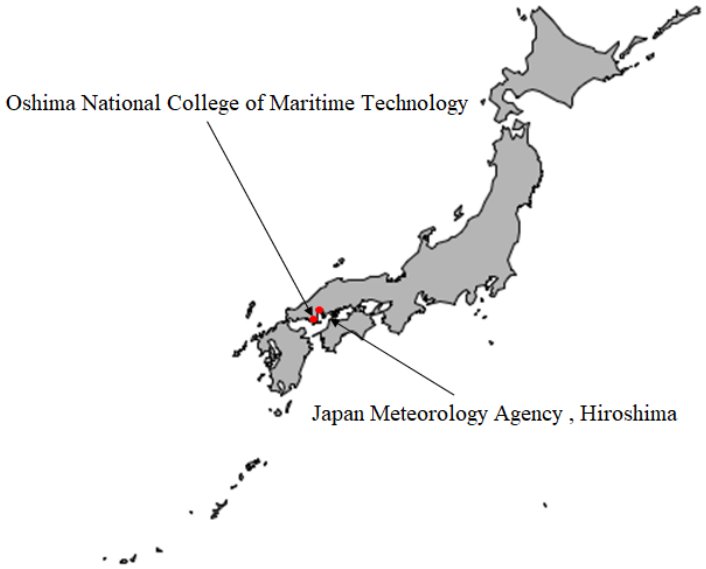


***Figure 1.*** *Locations of measurements: Oshima National College of Maritime Technology in Yamaguchi and Japan Meteorological Agency (JMA) in Hiroshima, Japan*

***Table 1.*** *Summary of the dates of the land measurements*

| *Seasons* | *Case No.* | *From (Date)* | *to (Date)* | *Number of rainy day(s)* |
|---|---|---|---|---|
| Summer | L-1 | July 18, 2019 | Jul 19, 2019 | 1.5 |
| | L-2 | Jul 22, 2019 | Jul 25, 2019 | 0 |
| | L-3 | Aug 3, 2019 | Aug 6, 2019 | 0 |
| Fall | L-4 | Oct 27, 2019 | Oct 29, 2019 | 1 |
| | L-5 | Oct 30, 2019 | Oct 31, 2019 | 0 |
| | L-6 | Nov 8, 2019 | Nov 10, 2019 | 1 |
| | L-7 | Nov 12, 2019 | Nov 14, 2019 | 1 |
| | L-8 | Nov 16, 2019 | Nov 19, 2019 | 0 |
| | L-9 | Nov 20, 2019 | Nov 23, 2019 | 1 |
| Winter | L-10 | Nov 29, 2019 | Dec 2, 2019 | 1 |
| | L-11 | Dec 5, 2019 | Dec 8, 2019 | 0 |
| | L-12 | Dec 26, 2019 | Dec 27, 2019 | 1.5 |
| | L-13 | Jan 15, 2020 | Jan 17, 2020 | 1 |

(Note) Condensation sensor is installed for only Case L-13.

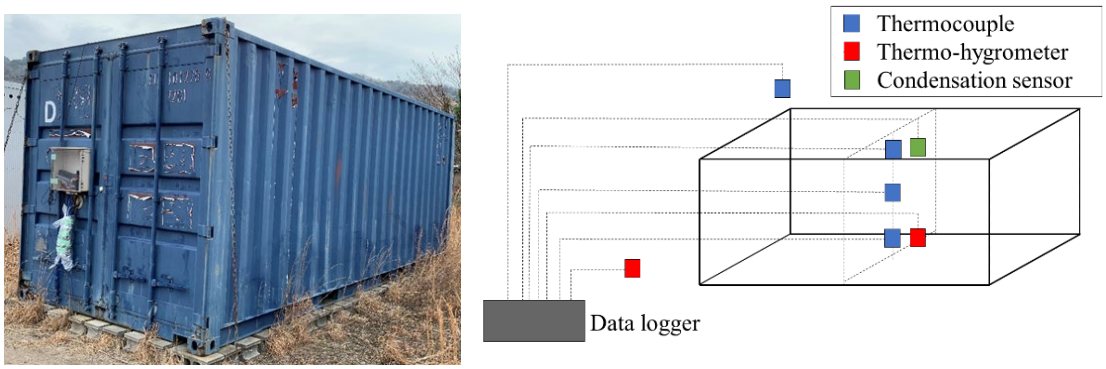


***Figure 2.*** *Photograph of the 20 ft dry box container used for the land measurements (left) and schematic of the set-up of the land measurements and locations of sensors and data logger (right)*

The container used in the land experiment was leased in collaboration with a Japanese maritime organization from the summer of 2019 to the winter of 2020. This rendered it difficult to carry out the land experiment during the spring season. The weather patterns of the spring season have been modified by applying the measured data from the fall season. Thus, future studies should ensure the accumulation of data during the spring season for more accurate results. The condensation inside a container is expected to occur empirically more in autumn, because the

internal dew point temperature and humidity are more favorable for the formation of water moisture. This is why land experiments were frequently carried out in autumn over other seasons, to analyze the weather conditions facilitating condensation.

### *3.2. Onboard measurements during navigation*

In the onboard measurements, it is ideal to install sensors inside for all the containers to monitor the situations during the voyage. However, this is not realistic, because the setting of nearly 20,000 sensors in each voyage seems impossible for various reasons. Although onboard measurements were difficult owing to the technical problem of data transfer at sea, onboard monitoring techniques have been developed in recent decades (Sasa et al., 2015; Sasa et al., 2017; Lu et al., 2017; Jing et al., 2021). In this study, we developed an onboard measurement system to monitor weather changes during the voyage on a newly built 20,000 TEU container vessel (see Figure 3) from May to December 2019. The vessel has a length of 400 m, breadth of 58.8 m, full loaded draft of 16.02 m and voyage speed of 22.8 knots.

***Figure 3.*** *Photograph of the 20,000 TEU container vessels used for the experiment*

In container transportation, the main shipping routes are the Trans-Pacific, Trans-Atlantic, and Asia–Europe routes. The voyage route of the 20,000 TEU container ship is between Far East Asia and Europe, as shown in Figure 4. The route goes through the East China Sea, South China Sea, Indian Ocean, Red Sea, Mediterranean Sea, and Atlantic Ocean, and it is connected with narrow waters such as the Malacca Strait, Suez Canal, Gibraltar Channel, and Dover Channel. The vessel completed three round trips between Qingdao, China, and Hamburg, Germany, from May to December 2019. The data measured on the vessel were collected at the end of December 2019 in Kaohsiung, Taiwan. Table 2 summarizes all ports of call and visiting dates. Unlike the Trans-Pacific or Trans-Atlantic routes, this voyage route goes through many continents. Air conditions during navigation are influenced by the effects of reflection, absorption, and radiation of heat, and these properties are much more complex in coastal areas than in the ocean. In other words, weather change is more sensitive near coastal regions. The measured weather parameters were the solar radiation, air temperature, humidity, sea water

temperature, and wind conditions, etc. A pyranometer and thermo-hygrometer were installed outside the bridge, which is the highest position of the vessel, as shown in Figure 5 (left and center). The cables were connected from the sensors to the power supply and data logger inside the bridge. The measured data related to the navigation and engine were sent to the voyage data recorder, which must be installed for all outbound vessels. An integrated bridge satellite system connected to the voyage data recorder was also installed inside the bridge to establish communication from vessel to land. As shown in Figure 5 (right), a laptop was connected to the integrated bridge satellite system to collect navigation data, such as position, speed course, steering angle, wind speed, and direction, which were recorded every second. The design of the onboard measurement system is illustrated in Figure 6.

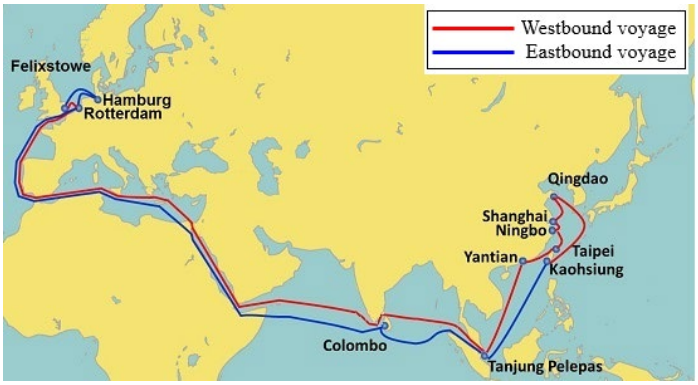


***Figure 4.*** *Voyage route of the container vessel, (Evergreen International Corp.)*

***Table 2.*** *Summary of the ports of call for the three round trips in 2019*

| *Date* | *Voyage 1* | *Date* | *Voyage 2* | *Date* | *Voyage 3* |
|---|---|---|---|---|---|
| May 12 | Qingdao | Jul 26 | Qingdao | Oct 11 | Qingdao |
| May 14 | Shanghai | Jul 28 | Shanghai | Oct 14 | Shanghai |
| May 16 | Ningbo | Jul 30 | Ningbo | Oct 15 | Ningbo |
| May 19 | Taipei | Aug 2 | Taipei | Oct 17 | Taipei |
| May 21 | Yantian | Aug 4 | Yantian | Oct 19 | Yantian |
| May 25 | Tanjung Pelepas | Aug 8 | Tanjung Pelepas | Oct 24 | Tanjung Pelepas |
| Jun 13 | Rotterdam | Aug 28 | Rotterdam | Nov 14 | Rotterdam |
| Jun 16 | Felixstowe | Aug 31 | Felixstowe | Nov 16 | Felixstowe |
| Jun 19 | Hamburg | Sep 4 | Hamburg | Nov 19 | Hamburg |
| Jun 22 | Rotterdam | Sep 8 | Rotterdam | Nov 22 | Rotterdam |
| Jul 11 | Colombo | Sep 26 | Colombo | Dec 16 | Colombo |
| Jul 15 | Tanjung Pelepas | Oct 3 | Tanjung Pelepas | Dec 23 | Tanjung Pelepas |
| Jul 21 | Kaohsiung | Oct 9 | Kaohsiung | Dec 29 | Kaohsiung |
| Jul 26 | Qingdao | Oct 11 | Qingdao | | |

***Figure 5.*** *Photographs of the pyranometer (left), thermo-hygrometer (center) outside the bridge and the devices for data storage inside the bridge (right)*

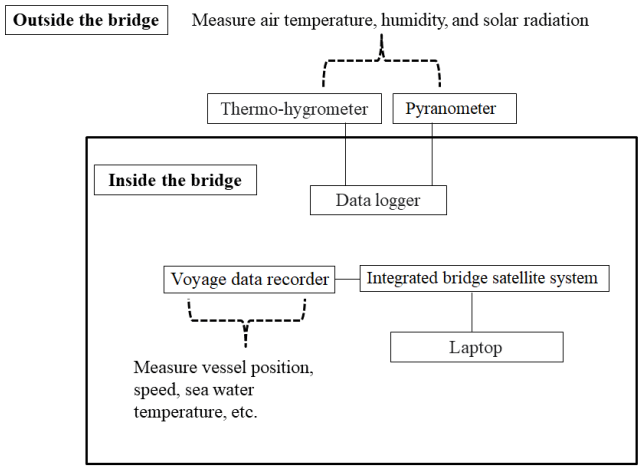


***Figure 6.*** *Set-up of the onboard measurement showing the locations of sensors and other recording devices inside and outside the bridge*

## 4. Land and onboard measurements results

### *4.1. Land measurement results*

The results of the measurements of the air temperature, humidity (inside and outside), and solar radiation for Cases L-3 (summer), L-6 (fall), and L-12 (winter) are shown in Figures 7, 8, and 9, respectively. It can be seen that the air temperatures inside the container are approximately 20–40 °C higher than those outside the container in every season. The humidity outside the container increases from night to morning slightly more than the humidity inside the container. The maximum values of the solar radiation in summer, fall, and winter were approximately 900, 600, and 420 W/m$^2$, respectively.

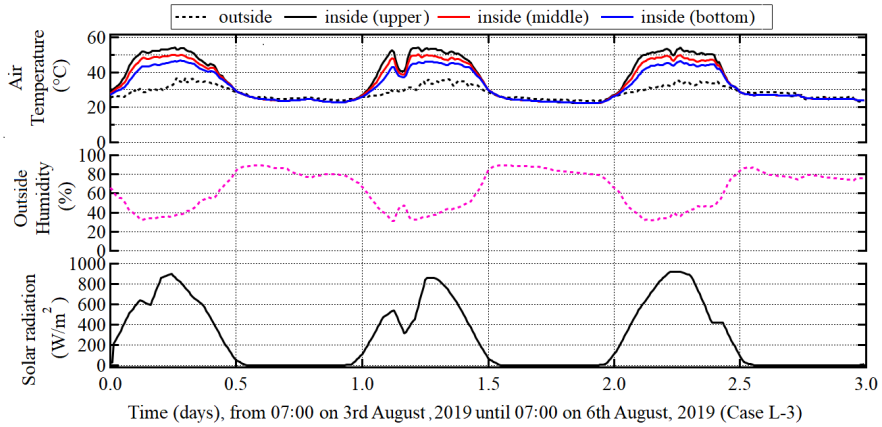


***Figure 7.*** *Land measurements of air temperatures (inside and outside), humidity (outside), and solar radiation in summer (Case L-3)*

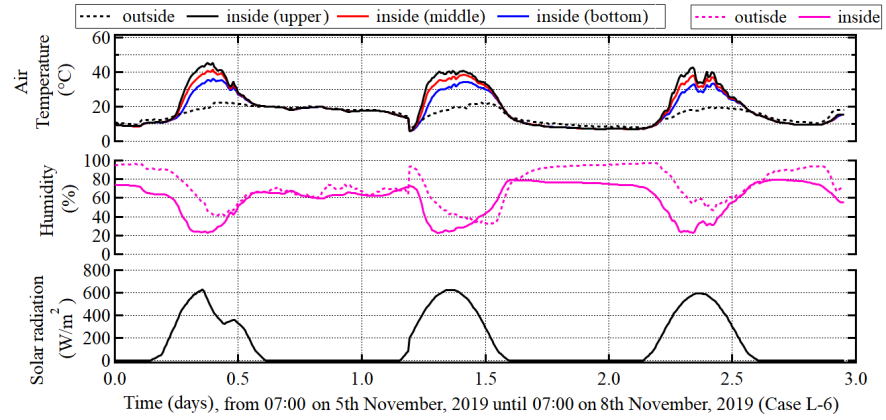


***Figure 8.*** *Land measurements of air temperatures (inside and outside), humidity (inside and outside), and solar radiation in fall (Case L-6)*

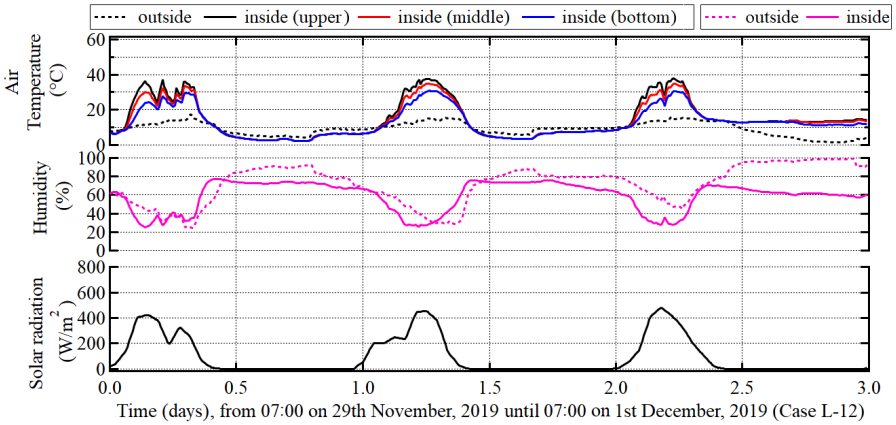


***Figure 9.*** *Land measurements of air temperatures (inside and outside), humidity (inside and outside), and solar radiation in winter (Case L-12)*

Figure 10 shows the maximum and minimum temperatures inside and outside the container in each season. It can be seen that the maximum air temperatures outside the container in Case L-3 (summer), Cases L-4 and L-5 (fall), and Case L-11 (winter) were 36, 25, 25, and 18 °C, respectively. The highest air temperature inside the container was always measured in the upper position, and exceeded 50, 45, and 40 °C in Case L-3 (summer), Cases L-4, 5, 6, 7, and 8 (fall), and Cases L-10 and 12 (winter), respectively. The minimum temperatures inside the container were comparable in all positions (upper, middle, and bottom) and were 20, 8, and −1 °C in summer, fall, and winter, respectively.

Figure 11 shows the measurement results of the maximum and minimum humidity inside and outside the container in each season. It can be seen that the maximum and minimum humidity inside the container were approximately 80% and 20%, respectively, in Cases 4–12 (fall and winter). This trend was not observed in summer owing to data unavailability. It can also be seen that the humidity outside the container was 10%–20% higher than that inside the container. Furthermore, the minimum humidity outside the container in summer was slightly higher than those in fall and winter.

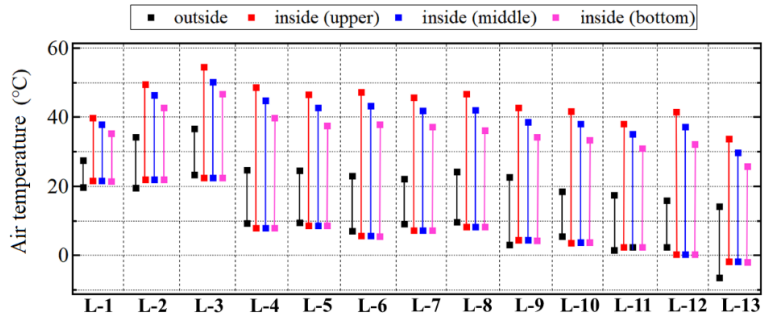


***Figure 10.*** *Land measurements of maximum and minimum temperatures outside and inside the container (upper, middle, and bottom parts)*

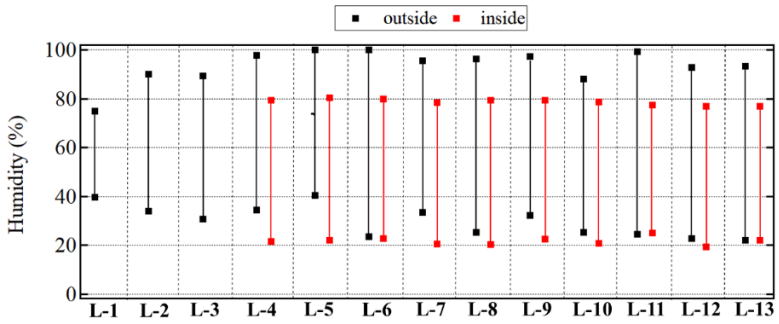


***Figure 11.*** *Land measurements of maximum and minimum humidity outside and inside the container*

### *4.2. Onboard measurement results*

In the westbound route, the ship departs from Qingdao, China (Day 1) at 36°N, passes through the Malacca Strait (Day 13) at 01°N, and arrives in Hamburg, Europe (Day 40) at 56°N. Then, the eastbound voyage starts from Europe to China on Day 40 and ends on Day 80. Figure 12 shows the latitudes for each voyage. From the figure, it can be seen that the maximum difference in latitude is 55°; owing to this large latitude difference, a significant variation in air conditions is expected over the forty-day voyage.

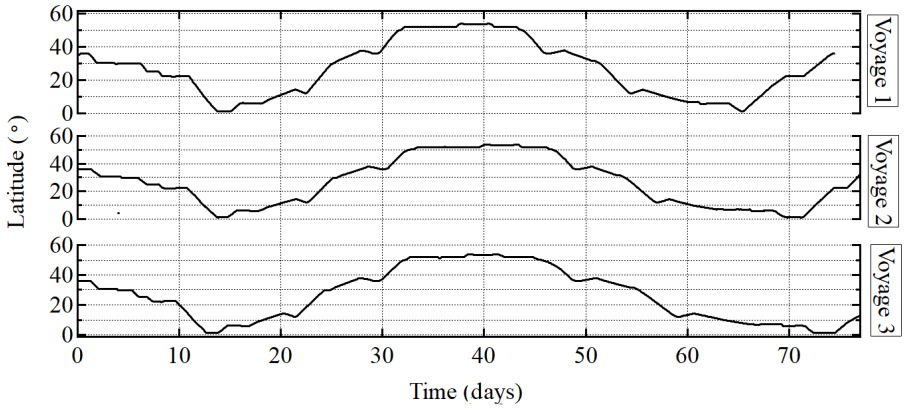


***Figure 12.*** *Latitudes of Voyages 1–3*

*4.2.1. Calculation of dew point temperature during navigation*

As mentioned in Section 2.1, we assumed that condensation occurs if Eq. (1) or (2) is satisfied. The dew point temperature can be calculated from the air temperature $T_a$ [°C] and relative humidity *R.H.* [%] as follows:

$$R.H. = \frac{P_w}{P_{ws}} \times 100 \ (\%), \tag{3}$$

where $P_w$[kPa] is the vapor partial pressure, and $P_{ws}$ [kPa] is the saturation vapor pressure, which is a function of the temperature. Among the various equations proposed to calculate $P_{ws}$ (Goff-Gratch, 1957; Teten, 1967; Magnu, 1995; Buck, 1981), Tenten's equation is the most frequently used (Verhoef et al., 2006; Gao et al., 2008):

$$P_{ws} = 0.61078\exp\left(\frac{17.27t}{t+237.3}\right). \tag{4}$$

Substituting Eq. (4) into Eq. (3) and rearranging the formula, the dew point temperature $T_{dp}$ [°C] can be expressed as follows:

$$T_{dp} = \left( \frac{237.3A}{17.27-A} \right), \quad (5)$$

where $A$ is a coefficient calculated by

$$A = \ln R.H. + \left(\frac{17.27T}{T+237.3}\right). \quad (6)$$

Air temperature, humidity, and direct sunlight can be considered as the primary factors influencing the internal air conditions of the container. The relationship of these factors with condensation was analyzed, as described in the subsequent section. Sea water temperature was also included in the analysis because of its close relationship with the air temperature. The comparison of these factors helps to develop a good understanding of how air temperature changes with sea water temperature in an actual sea. Although the sea water temperature also influences the air conditions of containers stowed in a cargo hold, sufficient data regarding the distribution of air temperatures or solar radiation have not been collected, which needs to be considered in future studies.

*4.2.2. Air temperature, sea water temperature, and dew point temperature*

Figure 13 shows the air temperature, sea water temperature, and dew point temperature measured in Voyages 1–3. The dew point temperature in the outside air was calculated using Eqs. (5) and (6) based on the outside air temperature and humidity. The difference in air temperature was approximately 15 °C between Qingdao and the Indian Ocean (Days 1–10) in Voyage 1 (spring) and Voyage 3 (fall). However, in Voyage 2, the air temperature was maintained at approximately 30 °C on Days 1–20 (summer). This implies that the seasonal difference in air temperature becomes larger and more significant at higher latitudes. On the other hand, the air temperature remains almost constant throughout the year in tropical regions, such as the Indian Ocean. The air temperature is slightly lower in Voyages 2 and 3 than in Voyage 1 over the Indian Ocean. The measured data show that the air temperature was approximately 30 °C when the ship passed through the Indian Ocean on Days 13–21 and 57–67 in Voyages 1–3. The air temperature was constant until the ship passed through the Suez Canal (Days 20–25) in each case. Over the Mediterranean Sea, the air temperature drops significantly towards the Gibraltar Channel and the Atlantic Ocean. The difference in air temperature is approximately 15–25 °C from the Mediterranean Sea to the Atlantic Ocean (Days 23–32 and Days 46–55). The difference in temperature between Europe and the Indian Ocean tends to increase in Voyage 3 (winter) compared to Voyages 1 and 2. It is obvious that the ship encounters two significant changes in air temperatures over long periods of approximately 10 days, and this change in meteorological conditions can influence container

condensation. In addition, some large, short-period variations of around one day were observed on Days 25–55. It is also shown that the sea water temperature is very close to the air temperature during most of Voyages 1–3, except on Days 35–50 (Europe) in Voyages 2 and 3. This implies that the long-period variations in air temperature and sea water temperature are strongly related to each other. The dew point temperature of the outside air is 2–5 °C lower than the air temperature in all the voyages.

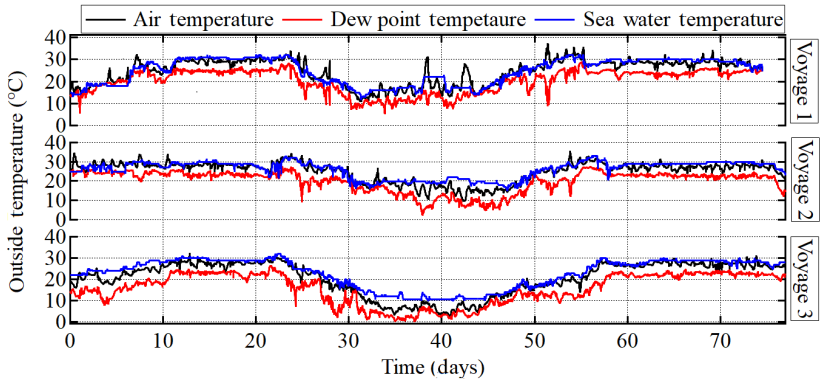


***Figure 13.*** *Onboard measurements of air temperature, sea water temperature, and dew point temperature in Voyages 1–3*

*4.2.3. Solar radiation*

Figure 14 shows the variation in solar radiation in Voyages 1–3. In the Indian Ocean (Days 13–21 and Days 57–67), in all voyages, although low levels of solar radiation are expected during rainy or cloudy days, only negligible variation was generally observed at low latitudes. The maximum values of solar radiation in the Indian Ocean in Voyages 1–3 were 1,000–1,200 W/m$^2$. In contrast to the Indian Ocean, a remarkable decrease in solar radiation was observed over Europe and Far East Asia. Over Europe (Days 35–50), the maximum values of solar radiation in Voyages 1, 2, and 3 were 1,020, 900, and 220 W/m$^2$, respectively. In Far East Asia (Days 1–10 and 67–80), the maximum values of solar radiation in Voyages 1, 2, and 3 were 1,040, 1,100, and 900 W/m$^2$, respectively. Although the decrease over Far East Asia in Voyage 3 is not significant compared to that over Europe, the solar radiation tends to decrease more significantly during the winter season in higher-latitude regions. In particular, the solar radiation may influence the long-term variations in air temperature and sea water temperature.

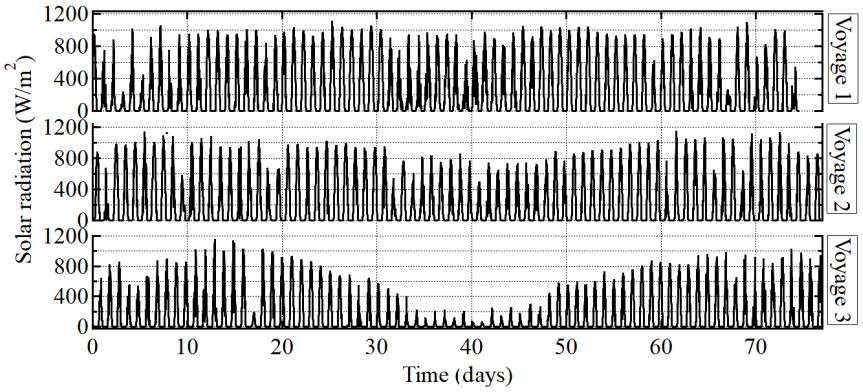


***Figure 14.*** *Onboard measurements of solar radiation in Voyages 1–3*

*4.2.4. Humidity and water vapor pressure*

Figure 15 shows the measurements of the humidity in Voyages 1–3. Over the Indian Ocean (Days 13–21 and 57–67), humidity was maintained at approximately 60%–90% On the other hand, a humidity of over 95% was measured in Europe (Days 35–50) in Voyages 1 and 3 and in Far East Asia (Days 1–10 and Days 67–80) in Voyages 1 and 2. In addition, significant short-term variations were observed in Europe and Far East Asia. In Europe, the largest daily variations were found to be from 24% to 90% and from 38% to 80% in Voyages 1 and 2, respectively. In Far East Asia, the largest daily variations were found to be from 42% to 98% and from 42% to 88% in Voyages 1 and 2, respectively.

Figure 16 shows the water vapor pressure in Voyages 1–3 calculated using Eqs. (5) and (6) based on the air temperature and humidity measurements. A higher humidity is measured over Europe than the Indian Ocean, while the water vapor pressure shows the opposite trend. The water vapor pressure over the Far East Asia and the Indian Ocean was approximately 2 and 3 kPa, respectively, in all voyages. However, in Europe, the water vapor pressure decreased from approximately 1.5 to 0.5 kPa from Voyage 1 to Voyage 3. This shows that the water vapor pressure in Europe decreases obviously from summer to winter. This also indicates that the water vapor content may be higher at lower latitudes than at higher latitudes. These results indicate that the water vapor pressure changes more in a long period than humidity. Although humidity is higher at higher latitudes, this tendency is not strong. Because the water vapor pressure is an indicator of the actual moisture content in the air, it was selected for the estimation of the condensation in this study.

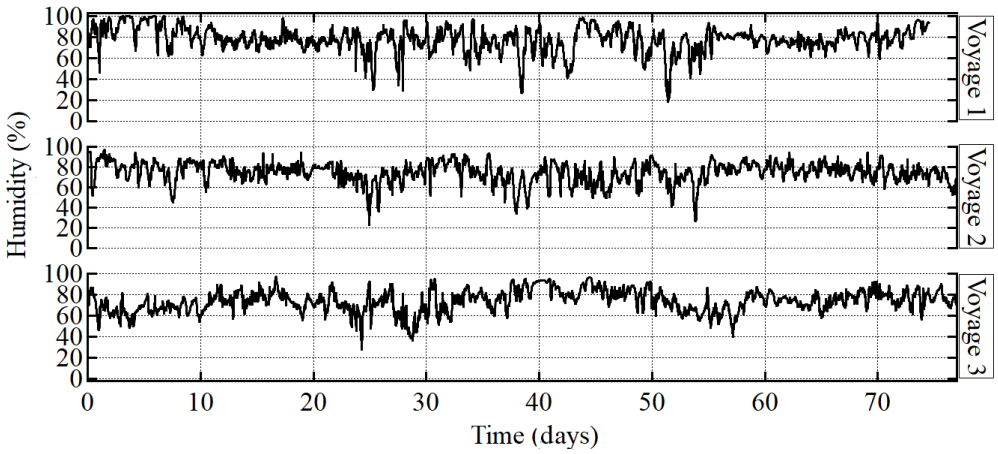


***Figure 15.*** *Onboard measurements of humidity in Voyages 1–3*

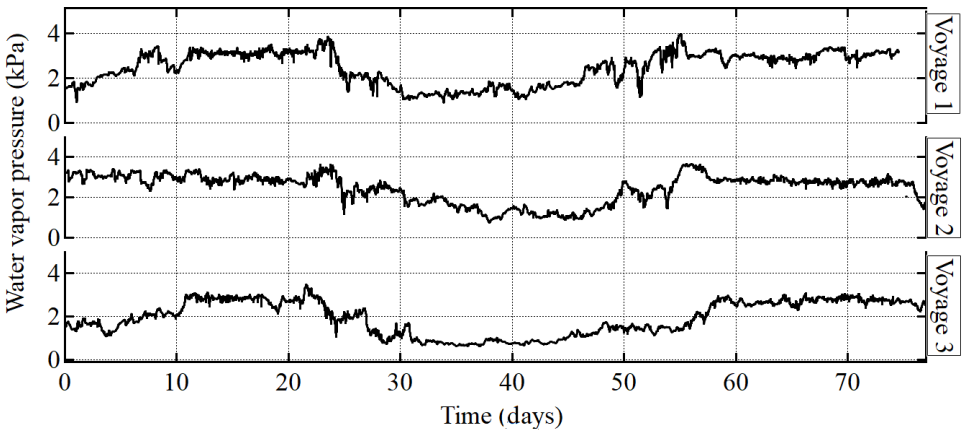


***Figure 16.*** *Calculation results of water vapor pressure in Voyages 1–3*

### *4.3. Statistical analysis of measured parameters*

#### *4.3.1. Correlation analysis of land measurements*

A correlation analysis was conducted to determine the relationship between the outside and inside air conditions. Figures 17, 18, and 19 show plots of the inside temperature as a function of the solar radiation, outside temperature, and outside humidity, respectively. The absolute values of the correlation coefficient are found to be approximately 0.8–0.9, indicating strong relationships. Figure 20 shows plots of the inside temperature as a function of the outside water vapor pressure. The absolute values of the correlation coefficient in each season are found to be approximately 0.10–0.49. In summer, the water vapor pressure varies around 1.5–3.4 kPa, and the inside temperatures tend to increase when the outside water vapor pressure decreases. This tendency is not clearly observed in fall and winter; the variation in water vapor pressure decrease to approximately 0.5–1.5 kPa in fall and 0.5–1.0 kPa in winter.

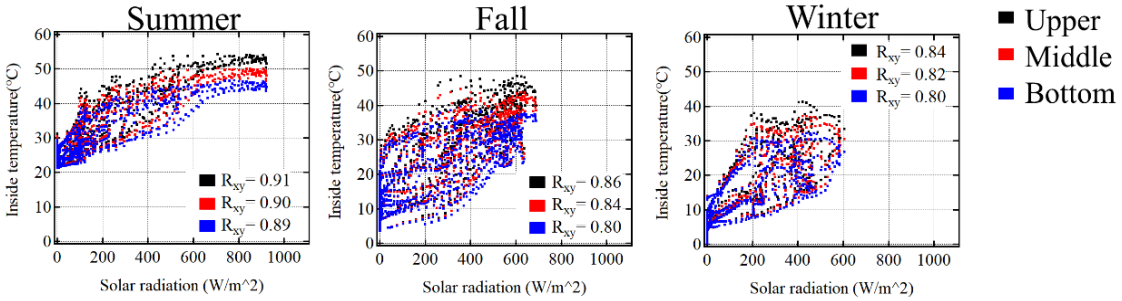


***Figure 17.*** *Relations of inside temperature as a function of the solar radiation in summer (left), fall (middle), and winter (right)*

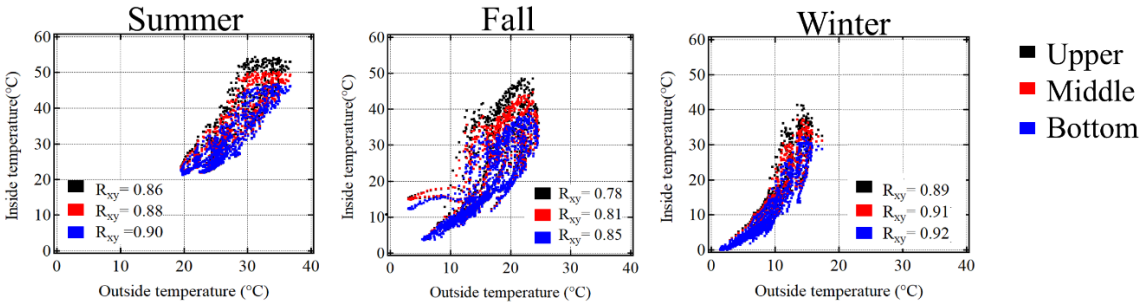


***Figure 18.*** *Relations of inside temperature as a function of the outside air temperature in summer (left), fall (middle), and winter (right)*

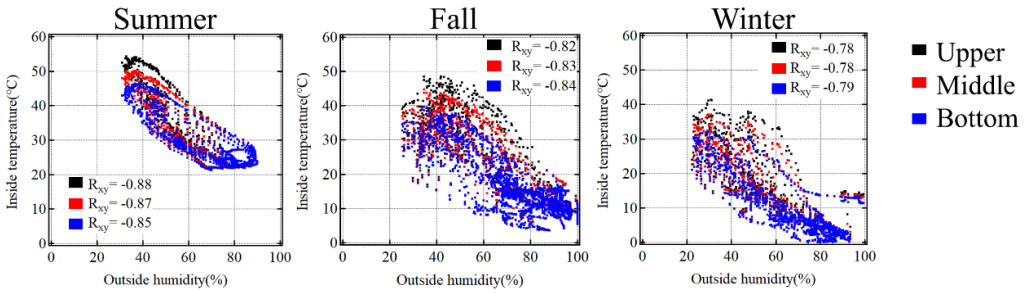


***Figure 19.*** *Relations of inside temperature as a function of outside humidity in summer (left), fall (middle), and winter (right)*

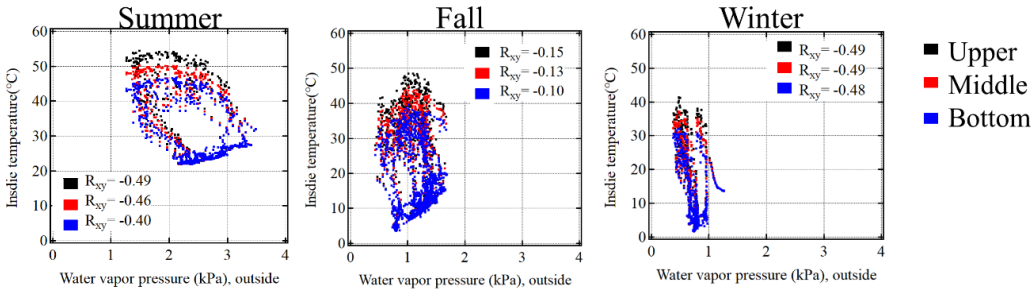


***Figure 20.*** *Relations of inside temperature as a function of outside water vapor pressure in summer (left), fall (middle), and winter (right)*

*4.3.2. Correlation analysis of onboard measurements*

The outside air conditions vary significantly because the ship moves across different sea areas with large differences in latitude (55°) between the Malacca Strait and Port of Hamburg, Germany. Figure 21 shows plots of the air conditions as functions of the latitude. The correlation coefficients are found to be −0.80, −0.77, and −0.93 in Voyages 1, 2, and 3, respectively. This shows that the air temperature is strongly influenced by the position of the ship, especially the latitude. The air temperature showed little change at low latitudes (0–15°N, Indian Ocean). On the other hand, it varied significantly at latitudes higher than 40°N, especially in Voyage 3. Furthermore, it is worth noting that the water vapor pressure shows a similar variation with the air temperature, with high correlation coefficient of −0.84, −0.77, and −0.95 in Voyages 1, 2, and 3, respectively. On the other hand, the solar radiation and humidity are less correlated with the latitude than with the air temperature and water vapor pressure. However, it suddenly dropped at 30°N near the Red Sea and the Suez Canal. A similar phenomenon was observed at 53°N near the port of Hamburg, Germany. It is worth noting that the former case occurs in coastal areas, and the latter occurs in an inland port. This indicates that the air condition is sensitive because different values of thermal capacity in land and sea influence each other, as mentioned in the field of meteorology (Kondo, 2004).

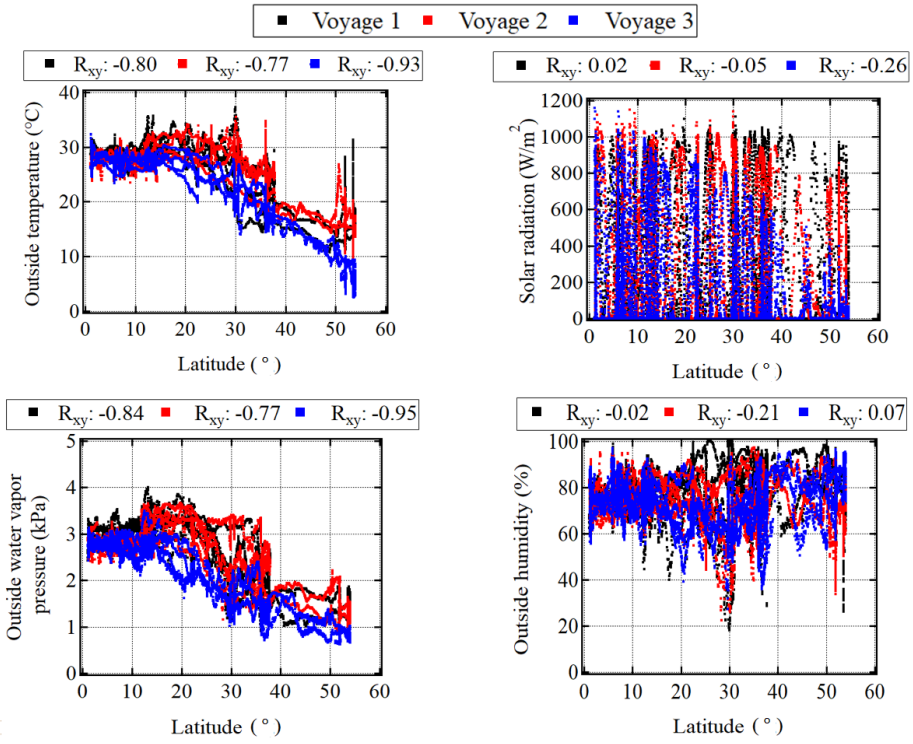


***Figure 21.*** *(top-left) Outside temperature, (top-right) solar radiation, (bottom-left) outside water vapor pressure, and (bottom-right) outside humidity as functions of the latitude in Voyages 1–3*

## 5. Multi regression modelling and estimation results

### *5.1. Multi regression modelling*

The air temperature and water vapor pressure inside the container were estimated with multi regression models. Eq. (7), defined as Model I, shows that multi regression formulae consist of three explanatory variables, $x_1$, $x_2$, and $x_3$, which represent the external air temperature, external water vapor pressure, and solar radiation in this study, respectively; $T_1$, $T_2$, and $T_3$ denote the air temperatures inside the container at the upper, middle, and bottom locations, respectively; $W_p$ is the water vapor pressure inside the container, and $\beta_0$, $\beta_1$, $\beta_2$, and $\beta_3$ are the corresponding regression coefficients. The accuracy of Model I was the highest, so the other models were not used in this study.

| Model Number | Model Equation | |
|---|---|---|
| I | $T_1 = \beta_0 + \beta_1 x_1 + \beta_2 x_2 + \beta_3 x_3$<br>$T_2 = \beta_0 + \beta_1 x_1 + \beta_2 x_2 + \beta_3 x_3$<br>$T_3 = \beta_0 + \beta_1 x_1 + \beta_2 x_2 + \beta_3 x_3$<br>$W_p = \beta_0 + \beta_1 x_1 + \beta_2 x_2 + \beta_3 x_3$ | (7) |

*5.1.1. Data adjustment for summer season*

Before the multi-regression analysis, the following data adjustments were made. First, the data measured on rainy days (see Table 1) were excluded because the patterns of rain are complicated and reduce the estimation accuracy. The results of the land experiment included data for some rainy days, and it is difficult to model such conditions because of the limited amount of data. The percentage of sunny days was dominant in three voyages between the Far East Asia and Europe in 2019. Thus, the statistical models were constructed by excluding the rainy days in the land experiment. Second, the data are adjusted in Cases L1–L3 (summer) because the land measurement is not continuously conducted throughout the year, and there is a time gap of three months between summer and fall seasons. Hence, data measured on 28 October, 2019 (Case L-4), which is the earliest measurement in fall, were added to adjust the time period of the summer season to fill this time gap. We believe that this adjustment of data was necessary because no land experiments were carried out in September. To reflect the change in the weather conditions from August to September, the method of data supplement was used.

*5.1.2. Regression modelling of inside air temperatures and inside water vapor pressure*

Figure 22 shows the coefficient of determination $R^2$ results with regression Model I for the inside air temperature (upper level) and inside water vapor pressure. Other $R^2$ values of the inside air temperatures (middle and bottom levels) are not shown here because they are similar to those in the upper level. From the figure, it can be seen that Model I had the highest $R^2$, with values of 0.96, 0.94, and 0.88 in summer, fall, and winter, respectively. This indicates that estimation should be conducted using three explanatory variables.

Regression models for water vapor pressure show similar trends to those for the inside air temperature. The $R^2$ values of Model I were 0.95 and 0.81 in fall and winter, respectively. In Model I, the inside air temperatures and water vapor pressure in summer, fall, and winter were calculated using Eqs. (8), (9), and (10), respectively.

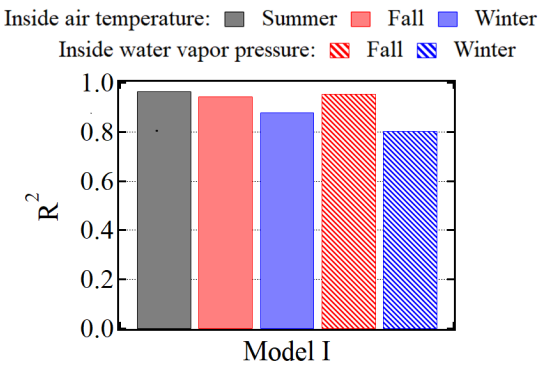


***Figure 22.*** *$R^2$ of Model I for the inside air temperature and inside water vapor pressure*

$$
\begin{aligned}
T_{1,summer} &= 13.68 + 1.09x_1 - 1.99 \times 10^{-1}x_2 + 1.62 \times 10^{-2}x_3 \\
T_{2,summer} &= 13.12 + 1.05x_1 - 1.80 \times 10^{-1}x_2 + 1.16 \times 10^{-2}x_3 \\
T_{3,summer} &= 11.46 + 1.03x_1 - 1.54 \times 10^{-1}x_2 + 7.19 \times 10^{-3}
\end{aligned} \tag{8}
$$

$$
\begin{aligned}
T_{1,fall} &= 7.60 + 8.88 \times 10^{-1}x_1 - 9.33 \times 10^{-2}x_2 + 4.72 \times 10^{-2}x_3 \\
T_{2,fall} &= 7.48 + 9.07 \times 10^{-1}x_1 - 9.34 \times 10^{-2}x_2 + 3.75 \times 10^{-2}x_3 \\
T_{3,fall} &= 6.74 + 9.56 \times 10^{-1}x_1 - 9.04 \times 10^{-2}x_2 + 2.53 \times 10^{-2}x_3 \\
W_{p,fall} &= 1.42 + 5.53 \times 10^{-2}x_1 - 7.58 \times 10^{-2}x_2 - 1.83 \times 10^{-3}x_3
\end{aligned} \tag{9}
$$

$$
\begin{aligned}
T_{1,winter} &= 9.88 + 4.07 \times 10^{-1}x_1 - 9.60 \times 10^{-2}x_2 + 5.72 \times 10^{-2}x_3 \\
T_{2,winter} &= 1.05 + 4.10 \times 10^{-1}x_1 - 1.02 \times 10^{-1}x_2 + 4.69 \times 10^{-2}x_3 \\
T_{3,winter} &= 1.12 + 4.16 \times 10^{-1}x_1 - 1.10 \times 10^{-1}x_2 + 3.45 \times 10^{-2}x_3 \\
W_{p,winter} &= 9.84 \times 10^{-1} + 2.85 \times 10^{-2}x_1 + 25.53 \times 10^{-1}x_2 - 1.62 \times 10^{-3}x_3
\end{aligned} \tag{10}
$$

### *5.2. Estimation of inside air conditions during navigation*

Air conditions inside each container during navigation were estimated using multiple regression formulas. It has been shown that three parameters (outside air temperature, outside water vapor pressure, and solar radiation) strongly influence the air conditions inside the container. However, the solar radiation and outside air temperature of the container are different at different locations on the ship because they depend on the direction of sunlight. In onboard measurements, outside air conditions were measured only on the bridge of the ship. Considering these facts, the condensation is discussed for containers with direct solar radiation, i.e., at the highest position, left-most, and right-most positions on the deck. According to the Köppen-Geiger climate classification (Kottek et al., 2006), the world map can be classified into different climate regions based on the global temperature and precipitation data sets. Based on this classification, the voyage route of the container ship between China and Europe can be divided into 6 different climate regions. To fully apply this classification, it was necessary to conduct the land experiments in each of these climate regions. However, in this study, land experiments were only carried out in Japan, owing to the large spatial scale and a limited budget; therefore, a simplified classification was applied by dividing the voyage into three different regions (east, middle, and west) as shown in Figure 23. In this simplified classification, the Indian Ocean and South China Sea both belong to the equatorial climate region and can therefore be defined as the middle region. On the other hand, the Mediterranean Sea, Atlantic Ocean, and Europe exhibit a similar characteristic of warm temperate climate and can therefore be defined as the west region. Finally, considering the latitude and temperature difference, the East China sea can be regarded as the east region despite a similar climatic classification to that of Europe in this study. Table 3 summarizes the regression equations used for each region. In the east region, Eq. (9) was applied to the westbound Voyage 1 (spring) owing to the lack of a

spring regression model.

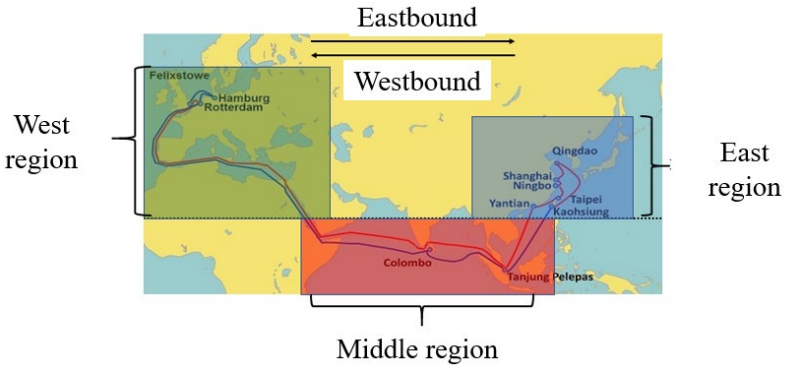


***Figure 23.*** *Definition of the east, middle, and west regions of the voyage*

***Table 3.*** *Selections of regression equations for parameter estimation during navigation*

| | | East | Middle | West |
|---|---|---|---|---|
| Voyage 1 | Westbound | Eq. (9) | Eq. (8) | Eq. (9) |
| | Eastbound | Eq. (8) | Eq. (8) | Eq. (9) |
| Voyage 2 | Westbound | Eq. (8) | Eq. (8) | Eq. (9) |
| | Eastbound | Eq. (9) | Eq. (8) | Eq. (9) |
| Voyage 3 | Westbound | Eq. (9) | Eq. (8) | Eq. (10) |
| | Eastbound | Eq. (10) | Eq. (8) | Eq. (10) |

The estimated results of the inside air temperatures in Voyages 1–3 are shown in Figures 24, 25, and 26, respectively. Figure 27 shows the inside temperature difference between the upper and bottom levels for all voyages. Figure 28 shows the outside humidity and the estimated inside humidity for all voyages. The inside humidity was obtained from the inside temperature (upper level) and inside water vapor pressure estimated using Eqs. (3) and (4), respectively; the inside dew point temperature was obtained from the inside humidity and inside air temperature in the upper level estimated using Eqs. (5) and (6), respectively.

*5.2.1. Estimated inside air temperatures and dew point temperatures*

From Figures 24 and 26, it can be seen that the maximum inside air temperature (upper level) increases from approximately 45 to 60 °C when the ship passes from Far East Asia to the Indian Ocean (Days 1–21) in Voyages 1 (spring) and 3 (fall). However, as shown in Figure 25, it remains between approximately 55 and 62 °C in Voyage 2 (summer). The maximum inside temperature (upper level) increases even more when the ship navigates from the Indian Ocean to the Mediterranean Sea with a large difference in latitude. The difference of the maximum

inside air temperature (upper level) between the middle and west regions is approximately 15 °C in Voyages 1 and 2. However, it increased to approximately 35 °C in Voyage 3. These results indicate that the latitude and season influence the inside air temperatures. The inside air temperatures change particularly when the ship navigates from low latitudes, such as the Indian Ocean, to high latitudes, such as Europe, in the winter season. It is worth noting that the inside air temperature (upper level) increased to almost 70 °C when the ship traveled across coastal seas near the Suez Canal, and to almost 60 °C inland ports of Europe in Voyage 1. The daily variation in the dew point temperature was approximately 12 °C in the middle region in all the voyages and in the east region in Voyage 2 (summer). However, this variation became smaller at high latitudes. In Europe, the daily variation was only approximately 5 °C in all voyages. Furthermore, the inside air temperatures were almost the same as the dew point temperature in Voyage 3 (winter) in Europe. This indicates that there is a high probability of container condensation during that time period. It can be observed that latitudes and seasons also influence the difference in the inside air temperatures between the upper and bottom levels, as shown in Figure 27. The difference is approximately 15–20 °C in all the voyages when the ship is in the Indian Ocean (Days 13–21 and Days 57–67). However, the difference becomes smaller at higher latitudes. In Europe (Days 35–50), the difference in Voyages 1, 2, and 3 is approximately 12, 10, and 2 °C, respectively. In Far East Asia (Days 1–10 and 67–80), the difference is similar to that in the Indian Ocean in Voyage 2 (summer), but it decreased to 2–10 °C in Voyages 1 (spring) and 3 (fall).

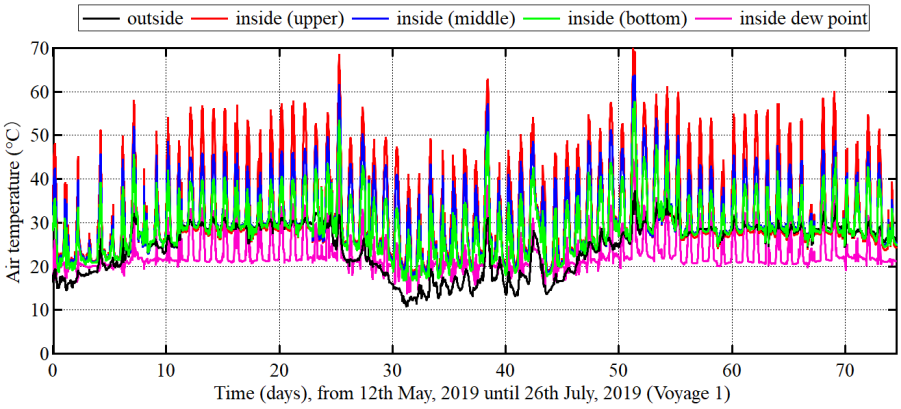


***Figure 24.*** *Variations in the estimated inside temperatures, dew point temperature, and humidity in Voyage 1*

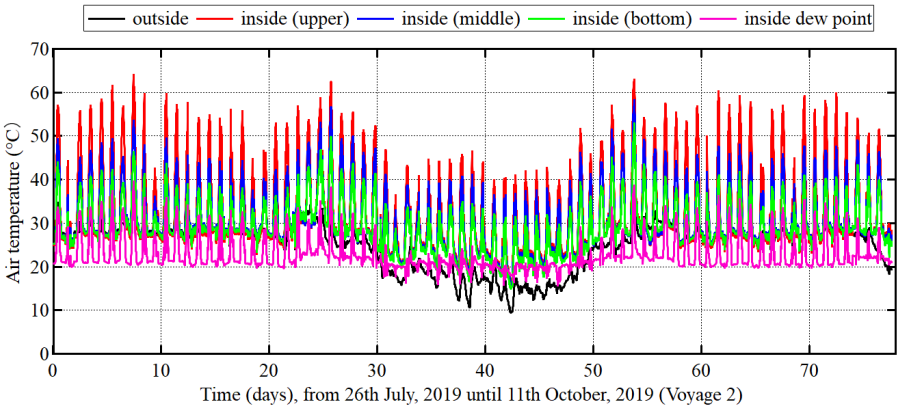


***Figure 25.*** *Variations in the estimated inside temperatures, dew point temperature, and humidity in Voyage 2*

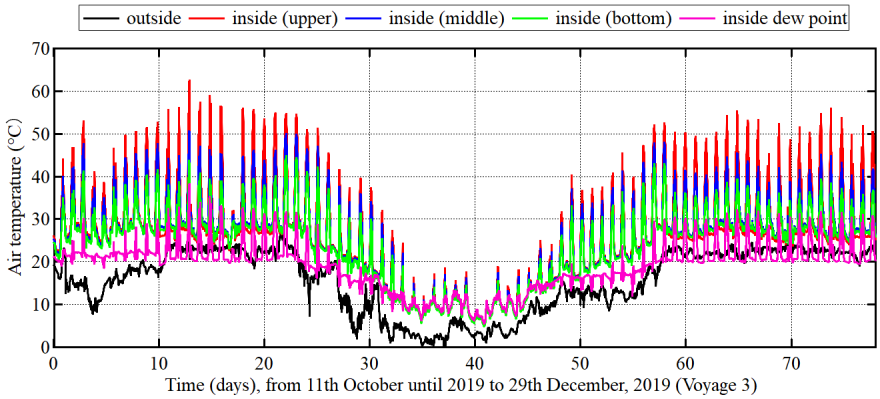


***Figure 26.*** *Variations in the estimated inside temperatures, dew point temperature, and humidity in Voyage 3*

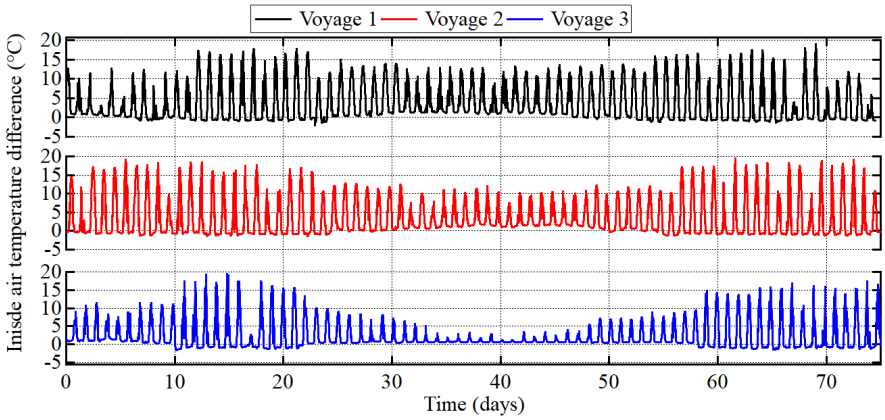


***Figure 27.*** *Variations in the inside air temperature difference between upper and bottom level in all voyages*

*5.2.2. Estimated inside humidity*

As shown in Figure 28, the inside humidity is also influenced by the latitude and season. First, the inside humidity tends to be higher at higher latitudes. When the ship travels across the Indian Ocean (Days 13–21 and 57–67), the maximum humidity remains approximately 70%–80% in all voyages. However, it increases to 95%–100% when the ship is in Europe (Days 35–50) in Voyages 1 and 2. The inside humidity in Europe during winter in Voyage 3 is higher than in Voyages 1 (summer) and 2 (fall). During Days 35–50, the humidity reaches 95%–100% after approximately 1, 1.3, and 8 days in Voyages 1–3, respectively. In Far East Asia (Days 1–10 and 67–80), the inside humidity remains approximately 90% in Voyage 1 (spring) and decreases to approximately 70%–80% in Voyages 2 (summer) and 3 (Fall). This tendency is similar to that of the outside humidity discussed in Section 4.2.

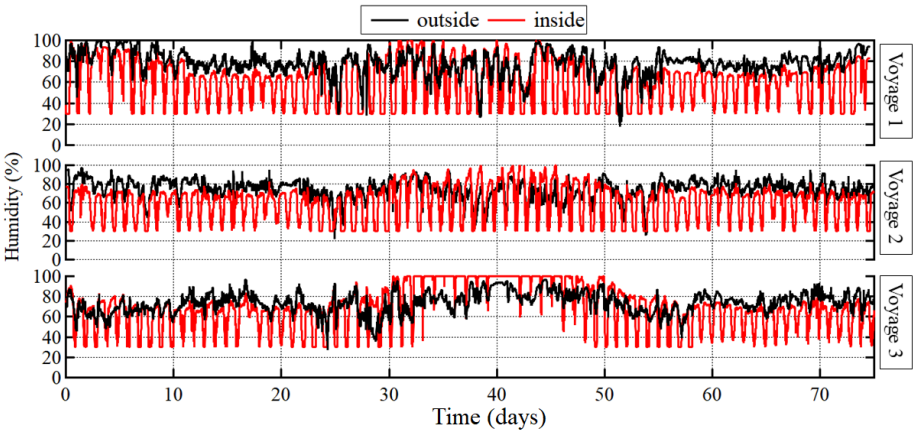


***Figure 28.*** *Variations in the estimated inside and outside humidity in all voyages*

*5.2.3. Comparison of estimated results with land measurement*

In this section, we compare the inside air conditions estimated by the multi-regression model with the land measurements. As reported in Section 4.1, the inside air temperature (upper level) measured on land in summer, fall, and winter is approximately 55, 40, and 38 °C, respectively. The results obtained using Eqs. (8) and (9) are similar to these land measurements. However, in Europe (Voyage 3), the estimated inside air conditions are very different from the land measurements in winter owing to the higher latitude. The estimated inside temperatures using Eq. (10) are smaller than those for the land measurements. The difference in the inside air temperature (upper level) over Europe and on land in winter is approximately 20 °C. In addition, a significant difference between Europe and the land measurements was observed in the estimated inside humidity, which varied within approximately 20%–80% in fall and winter, as reported in Section 4.1. However, the estimated humidity was over 95% according to Eqs. (9) and (10) for all voyages in Europe. On the other hand, the estimated results and measurements were similar in the Indian Ocean, Far East Asia, and on land (Japan) in all voyages.

## 6. Calculation of condensation probability

### *6.1. Definition of condensation inside the container and condensation probability*

As mentioned in Section 2, condensation may occur inside the container if either of the following conditions is satisfied: $T_w < D_a$ and $D_i > T_a$. These conditions were checked with land measurements. Figure 29 shows the outside humidity, inside air conditions, and periods of condensation inside the container. In this paper, the difference between the inside air temperature $T_1$ (upper level) and the inside dew point temperature $D_i$ is defined as $T_d$. It is clear that condensation occurs when the inside humidity exceeds 70% and $T_d$ decreases below 8 °C. Based on these results, the condensation conditions can be summarized as follows:

$$T_d \leq 8 \text{ °C}, \tag{11}$$

$$H_i \geq 70\%, \tag{12}$$

where $H_i$ is the inside humidity. The condensation probability, $P_{con}$, in the actual sea is defined as

$$P_{con} = \frac{T_{con}}{T_{toal}} \times 100\%, \tag{13}$$

where $T_{con}$ is the period that satisfies Eqs. (11) and (12), and $T_{toal}$ is the voyage time from the loading port to the discharging port.

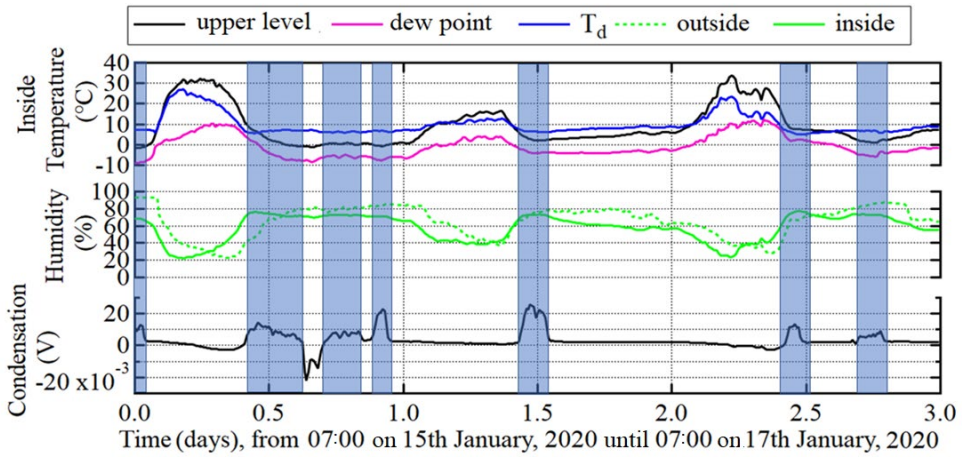


***Figure 29.*** *Variations in the inside air temperature, outside humidity, and condensation measured on land (L-13).*

*(Note) Blue area is the period of condensation.*

### *6.2. Calculation of condensation probability during navigation*

The probability of condensation, $P_{con}$, is estimated using Eq. (13) for certain patterns of the loading and discharging ports. The estimated results of $P_{con}$ are presented in Table 4, where Cases 1–3 refer to westbound voyages and Cases 4–6 refer to eastbound voyages. Figure 30 show the relationship between the latitude and $P_{con}$ in Cases 1 and 4, respectively. As shown in Figure 30 (left), $P_{con}$ increase steadily to 10%–20% in all the voyages when the ship travels from 36°N–0°. It then reaches 22%–25% before the ships enters the Dover Channel at approximately 49°N. In Voyages 1 and 2, $P_{con}$ increased to 38% and 32%, respectively, while in Voyage 3, it increased significantly from approximately 25% to 47% when the ship traveled at high latitudes in Europe. In Cases 2 and 3, $P_{con}$ was 50%–55% in Voyage 3, indicating that the ship may experience container condensations for nearly half of the total voyage time in the westbound voyage in winter, regardless of the loading ports. In Case 4 (Hamburg, Germany to Qingdao, China), $P_{con}$ in Voyages 1, 2, and 3 was estimated to be 27%, 38%, and 50%, respectively. As shown in Figure 30 (right), after the ship departs from Europe, $P_{con}$ increases to approximately 18%, 32%, and 45% from 54°N–0° in Voyages 1, 2, and 3, respectively. Then, $P_{con}$ increases by only 5%–10% in all voyages when the ship arrives at Qingdao, China. This indicates that the risk of condensation is higher during winter (Voyage 3) than during summer and fall (Voyages 1 and 2). In Case 5 (Colombo, Siri Lanka to Qingdao, China), $P_{con}$ was 30%–35% in all voyages. In Case 6 (Kaohsiung, Taiwan to Qingdao, China), $P_{con}$ decreased from 37% to 28% in Voyages 1 and 2. As shown in Figure 30 (right), the estimated inside humidity in Voyage 1 was approximately 70%–80% on Days 70–75 and remained constant at approximately 70% in Voyage 2 during the same period. Thus, $P_{con}$ in Case 6 is estimated to be higher in Voyage 1 than in Voyage 2. The estimated $P_{con}$ in Case 3 (Voyage 3) is not shown here because we only had measurements until Kaohsiung, Taiwan. $P_{con}$ is similar in westbound Voyages 2 and 3 and is slightly different in Voyage 1. On the other hand, $P_{con}$ is very different in all eastbound voyages. In the westbound voyages, $P_{con}$ increases by only 5%–7% in all voyages from 0° to 35°N. However, in the eastbound voyages, $P_{con}$ increases by approximately 5%, 20%, and 25% in Voyages 1, 2, and 3 from 35°N to 0°, respectively. This indicates that the probability of condensation is highest when the ship passes through the Indian Ocean and Mediterranean Sea and when the containers are loaded at higher latitudes, such as Europe, especially in fall and winter.

***Table 4.*** *Condensation probability $P_{con}$ in different loading and discharging ports*

| | Loading port | Discharging port | $P_{con}$ in Voyage 1 | $P_{con}$ in Voyage 2 | $P_{con}$ in Voyage 3 |
|---|---|---|---|---|---|
| Case 1 | Qingdao | Hamburg | 38% | 32% | 47% |
| Case 2 | Kaohsiung | Hamburg | 36% | 33% | 50% |
| Case 3 | Tanjung Pelaspas | Hamburg | 32% | 35% | 55% |
| Case 4 | Hamburg | Qingdao | 27% | 38% | 50% |
| Case 5 | Colombo | Qingdao | 35% | 30% | 32% |
| Case 6 | Kaohsiung | Qingdao | 37% | 28% | Nil |

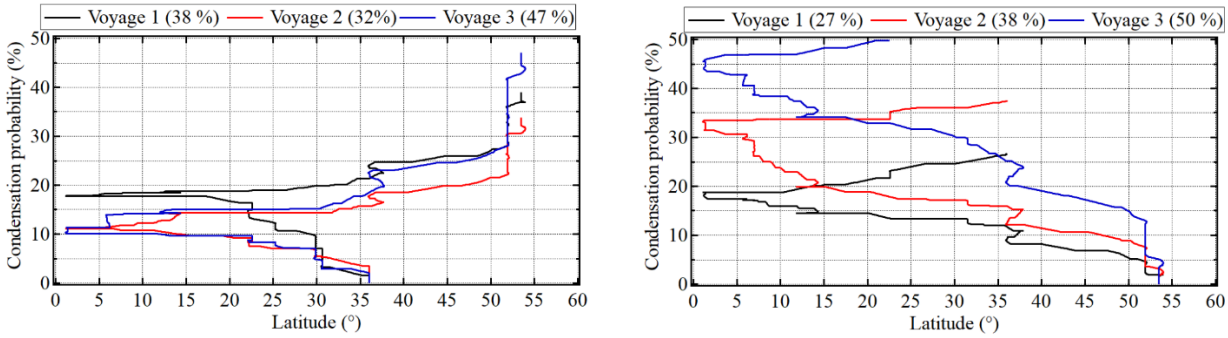


***Figure 30.*** *Condensation probability $P_{con}$ as a function of the latitude in Case 1 (Qingdao, China to Hamburg, Germany) (left) and Case 4 (Hamburg, Germany to Qingdao, China) (right) in the different voyages*

## 7. Conclusions

This study is defined as the first step to investigate the condensation within a dry box container by proposing a simple method. Simultaneously, onboard data are being collected presently to investigate the distribution of heat and temperature of each container for further studies. The main conclusions of this study are as follows.

(1) The land measurements revealed that the inside humidity does not vary significantly in fall and winter, and the air temperatures and solar radiation have significant variations throughout the year.

(2) The outside air conditions during navigation show complicated patterns owing to the large differences in latitude and the different meteorological conditions. This causes significant changes in outside air temperature, humidity, and solar radiation, especially during the winter season.

(3) In land, the inside temperature (upper level) was highly correlated with the solar radiation ($r_{xy}$=0.92), outside air temperature ($r_{xy}$=0.86), and outside humidity ($r_{xy}$=−0.88). During navigation, the latitude was highly correlated with the outside air temperature ($r_{xy}$= −0.80)

and the water vapor pressure ($r_{xy}$= −0.84).

(4) During navigation the water vapor pressure has a higher correlation with latitude than the humidity for the voyage route between Far East Asia and Europe. Hence, the outside water vapor pressure should be evaluated as a parameter in multi-regression analysis.

(5) It is shown that the inside air conditions should be estimated by the model with the following three explanatory variables: outside air temperature, water vapor pressure, and solar radiation.

(6) In land, condensation is found to occur if the absolute difference between the dew point temperature and air temperature inside the container is smaller than 8 °C and the inside humidity is higher than 70%. These conditions were applied to estimate the condensation probability for all voyages. The condensation probabilities are the highest in winter (Voyage 3), with a value of 47% and 50% in the westbound and eastbound voyages. This implies that the ship may encounter the air condition of condensation for almost half of the total period in containers with direct solar radiation.

(7) It was shown that the condensation probability remains at approximately 50% in Cases 1–3 during the winter season, especially in the westbound route, regardless of the loading ports. However, the condensation probability is lowered by 10%–20% if the container is loaded at lower latitudes, e.g., in Colombo, Sri Lanka, and Kaohsiung, Taiwan, in Cases 5 and 6 (Voyages 2 and 3).

(8) In the westbound voyages, variations of condensation probability were similar between Voyages 2 and 3 and were slightly different in Voyage 1. In the eastbound voyages, variations were very different in all voyages. The risk of condensation increased by 15%–20% when the ship passed through the Mediterranean Sea and the Indian Ocean and when containers were loaded at higher latitudes, such as Europe.

(9) The results of study show that container condensation is likely to occur in marine container transportation between Far East Asia and Europe. Nevertheless, we only investigate containers loaded on the deck with direct solar radiation owing to the limitations of the measured data. The condensation of containers in each location, including below the deck, must be studied by applying heat transfer theory with measured data in various positions of loaded containers. Furthermore, this problem should be considered as one of the new optimized parameters in the optimized ship routing analysis in future studies.

**Acknowledgements**

The authors wish to extend their gratitude to Shoei Kisen Kaisha Ltd., Imabari Shipbuilding Co., Ltd., and the crew of the 20,000 TEU container ship for their cooperation in conducting onboard measurements. The authors also express appreciation to UNIEX-NCT Corp. for

providing important information on container condensation. This study was financially supported by Challenging Research (Explanatory) (2018–2020, 18K1892, represented by Kenji Sasa) under a Grant-in-Aid for Scientific Research by the Japan Society for the Promotion of Science (JSPS).

**References**

**Accorsi, R., Manzini, R., Ferrari, E.** (2014). A comparison of shipping containers from technical, economic and environmental perspectives, *Journal of Transportation Research Part D*, **26**, pp.52-59. doi: 10.1016/j.trd.2013.10.009

**Alduchov, O.A., Eskridge RE.** (1995). Improved Magnus's form approximation of saturation vapor pressure, *Journal of Applied Meteorology*, **35**, pp.601-609. doi: 10.1175/1520-0450(1996)035<0601:IMFAOS>2.0.CO;2

**Ayyad, Z., Valli, E., Bendini, A., Accorsi, R., Manzini, R., Bortolini, M., Gamberi, M., Gallina Toshi, T.** (2017). Simulating international Shipments of Vegetables oils: Focus on quality changes, *Italian Journal of Food Science,* **29**, pp.38-49. doi: 10.14674/1120-1770/ijfs.v483

**Bijlsma, S.** (2008). Minimal Time Route Computation for Ships with Pre-Specified Voyage Fuel Consumption. *Journal of Navigation*, **61**(4), 723-733. doi:10.1017/S037346330800492X

**Borocz, P., Singh, P., Singh, J.** (2015). Evaluation of Distribution Environment in LTL Shipment between Central Europe and South Africa, *Journal of Applied Packaging Research*, **7** (2), pp.45-60. doi: 10.14448/japr.04.0003

**Buck, AL.** (1981). New equations for computing vapor pressure and enhancement factor, *Journal of Applied Meteorology*, **12**, pp.1527-1532. doi: 10.1175/1520-0450(1981)020<1527:NEFCVP>2.0.CO;2

**Castelein, B., Geerlings, H., Duin, R.V.** (2020). The reefer container market and academic research: A review study. *Journal of Cleaner Production*, **256,** doi: 10.1016/j.jclepro.2020.120654

**Chang, S.J., Wi, S., Kang, S.G., Kim, S. (2020).** Moisture risk assessment of cross-laminated timber walls: Perspectives on climate conditions and water vapor resistance performance of building materials, *Building and Environment,* **168**. doi: 10.1016/j.buildenv.2019.106502

**Chang, Y., Tseng, R., Chu, P., & Shao, H.** (2016). Global Energy-saving Map of Strong Ocean Currents. *Journal of Navigation*, **69**(1), 75-92. doi:10.1017/S0373463315000466

**Chou, M., Chou, T., Hsu, Y., & Lu, C.** (2017). Fuel Consumption Ratio Analysis for Transiting from Various Ports and Harbours in Asia through the Northern Sea Route. *Journal of Navigation*, **70**(4), 859-869. doi:10.1017/S0373463317000078

**Chiniforush, A.A., Valipour, H.R, Akbarnezhad, A.** (2019). Water vapor diffusivity of engineered wood: Effect of temperature and moisture content. *Construction and Building Materials,* **224**, 1040-1055. doi: 10.1016/j.conbuildmat.2019.08.013.

**Csavajda, P., Borocz, P.** (2019). Climate Conditions in ISO Container Shipments from Hungary to South Africa and Asia, *Periodica Polytechnica Transportation Engineering*, **3** (3), pp.233-241. doi: 10.3311/PPtr.11585

**Evergreen International Corp. Routing Network** (2019). *Routing network of China Europe Shuttle Service*. https://www.shipmentlink.com/tvs2/images/ces.jpg/. Accessed 2 January 2021.

**Excell, T.L., Stone, V.C.** (1989). Moisture Problems in the Shipment of Refined Sugar in Containers, *Proceedings of the South Africa Sugar Technologists' Association*, pp.68-72.

**Gao, J., Brewster K., Xue, M.** (2008). Variation of radio refractivity with respect to moisture and temperature and influence on radar ray path, *Advances in Atmospheric Sciences*, **25** (6), pp.1098-1106. doi: 10.1007/s00376-008-1098-x

**Goff, J.A.** (1957). Saturation pressure of water on the new Kelvin temperature scale, *Transactions of the American society of heating and ventilating engineers*, **63**, pp.347-354.

**Iejavs, J., Rozins, R.** (2016). Water vapor permeability properties of cellular wood material and condensation risk of composite panel wall. *ProLigno.* **12**, 3-11.

**Imaeda, Y. and Kubo, M., Hashimoto, T., Abe, T., Kiwaki, J.** (1971). On the Protection of Sweat Damage of Cargo in Container (1st Report), *Review of Kobe University of Mercantile Marine. Part II, Maritime studies, and science and engineering*, **18**, pp.191-204. (in Japanese)

**Imaeda, Y. and Kubo, M.** (1974). On the Protection of Sweat Damage of Cargo in Container (2nd Report), *Review of Kobe University of Mercantile Marine. Part II, Maritime studies, and science and engineering*, **22**, pp.295-308. (in Japanese)

**Jing, Q., Sasa, K., Chen, C., Yin, Y., Yasukawa, H., Terada, D.** (2021). Analysis of ship maneuvering difficulties under severe weather based onboard measurements and realistic simulation of ocean environment, *Journal of Ocean Engineering*, **221**. doi: 10.1016/j.oceaneng.2020.108524

**Kawahara, H., Kawakami, T., and Sasa, K.** (2020). Form of Condensation of Marine Dry Container Due to the Radiation Heat Transfer, *The Japan Society of Mechanical Engineers, The 58th General Meeting and Conference*, Hiroshima, Japan (in Japanese)

**Knowler, G.** (2019). *Global container growth forecast to rebound*. https:// www.joc.com/maritime-news/global-container-growthforecast_rebound_20190425.ht ml/. Accessed 12 January 2021.

**Kondo, J.** (2004). Meteorology of water environment—Heat and water balances on the surface—, *Asakura-Shoten*, pp.160-184. (in Japanese)

**Kottek, M., Grieser, J., Beck, C., & Rudolf, B.** (2006). World Map of the Köppen-Geiger climate classification updated. *Meteorologische Zeitschrift*, **15**(3), 259-263. doi:

10.1127/0941-2948/2006/0130

**Leinberger, D.** (2006). Temperature & Humidity in Ocean Containers, Proceedings of Dimensions.06. *International Safe Transit Association*, East Lansing, Michigan, USA.

**Levinson, M.** (2006). The Box: How the Shipping Container Made the World Smaller and the World Economy Bigger, Princeton University Press, pp.37.

**Lu, L.F., Sasa, K., Sasalo, W., Terada, D., Kano, T., Mizojiri, T.** (2017). Rough wave simulation and validation using onboard ship motion data in the Southern Hemisphere to enhance ship weather routing, *Journal of Ocean Engineering*, **144**, pp.61-77. doi: 10.1016/j.oceaneng.2017.08.037

**Maki, A., Akimoto, Y., Nagata, Y., Kobayashi, S., Kobayashi, E., Shiotani, S., Ohsawa, T., and Umeda, N.** (2011). A New Weather-Routing System that Accounts for Ship Stability Based on a Real-Coded Genetic Algorithm, *Journal of Marine Science and Technology*, **16**, pp.311-322. doi: 10.1007/s00773-011-0128-z

**Murray, FW.** (1967). On the computation of saturation vapor pressure, *Journal of Applied Meteorology*, **6**, pp.203-204.

**Palacios-Cabrera, H.A., Menezes, H.C., Iamanaka, B.T., Canepa, F., Teixeira, A.A., Carvalhaes, N, Santim D., Leme, P.T.Z., Yotsuyanagi, K., Taniwaki, M.H.** (2007). Effect of Temperature and Relative Humidity during Transportation on Green Coffee Bean Moisture content and Ochratoxin A Production, *Journal of Food Protection,* **70** (1), pp.164-171. doi: 10.4315/0362-028X-70.1.164

**Prpić-Oršić, J. and Faltinsen, O.M.** (2012). Estimation of Speed Loss and Associated CO2 Emissions in a Seaway, *Ocean Engineering*, **44**, pp.1-10. doi: 10.1016/j.oceaneng.2012.01.028

**Sasa, K., Tereda, D., Shiotani, S., Wakabayashi, N., Ikebuchi, T., Chen, C., Takayama, A., Uchida, M.** (2015). Evaluation of ship performance in international maritime tranportation using an onboard observation system-in case of a bulk carrier for international voyages, *Journal of Ocean Engineering*, **104**, pp.294-309. doi: 10.1016/j.oceaneng.2015.05.015

**Sharp, A.K, Fenner, Greve, J.E. Van S.** (1979). Prevention of condensation damage to Cocoa Beans shipped in containers, *Journal of Stored Products Research,* **15**, pp. 101-109.

**Shoji, R.** (2013). Element Technology on the Ship Weather Routing, *Operations Research*, **58** (10), pp.599-605. (in Japanese) doi: 10.1016/0022-474X(79)90005-5

**Singh, S.P., Singh, K.S.J., Sandhu, A.P.S.** (2012). Measurement and Analysis of Vibration and Temperature Levels in Global Intermodal Container Shipments on Truck, Rail and Ship, *Packaging Technology and Science*, **25**, pp.149-160. doi: 10.1002/pts.968

**Verhoef, A., Diaz-Espejo, A., Knight, JR., Garcial, VL., Fernandez, JE.** (2006). Adsorption of Water Vapor by Bare Soil in an Olive Grove in Southern Spain, *Journal of Hydrometeor,* **7** (5), pp.1011-1027. doi: 10.1175/JHM556.1

**Weiskircher, R.** (2008). Summary of Prior Experiments Regarding Temperature in Sea Containers A Literature Review by the Wine Supply Chain Council. *CSIRO Mathematical and Information Sciences*